Spontaneous network activity visualized by ultrasensitive Ca^{2+} indicators, yellow Cameleon-Nano

Kazuki Horikawa, Yoshiyuki Yamada, Tomoki Matsuda, Kentarou Kobayashi, Mitsuhiro Hashimoto,

Toru Matsu-ura, Atsushi Miyawaki, Takayuki Michikawa, Katsuhiko Mikoshiba & Takeharu Nagai
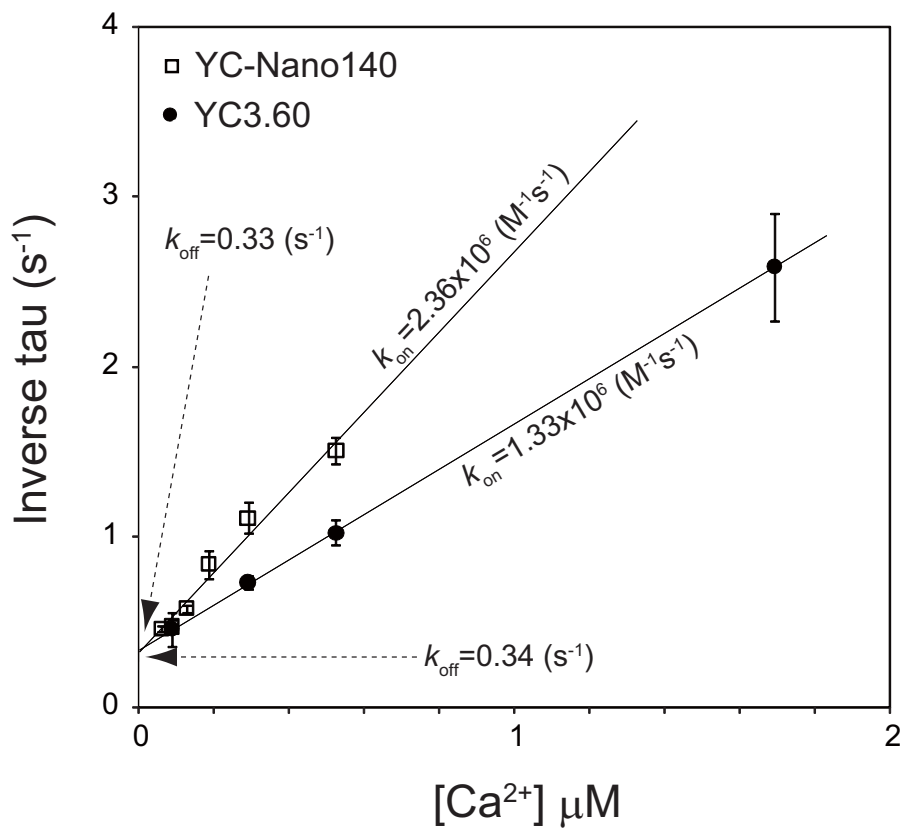
Supplementary figures and text:

Supplementary Figure 1	Ca^{2+} affinity of the YC-Nano.
Supplementary Figure 2	Relaxation rate constant (k_{obs}) for YC3.60 or YC-Nano140 with Ca^{2+}.
Supplementary Figure 3	Spectra for YC-Nano15.
Supplementary Figure 4	Growth rate and developmental time course of *D. discoideum* cells expressing YC2.60 and YC-Nano15.
Supplementary Figure 5	Ca^{2+} imaging of spontaneous network activity in a 100,000-cell network.
Supplementary Figure 6	Aggregation waves of *Dictyostelium* cells visualized with YC2.60.
Supplementary Figure 7	YC3.60 and YC-Nano15 signals in response to trains of action potentials.
Supplementary Table 1	Properties of new YC variants
Supplementary Table 2	Electrophysiological properties of layer 2/3 pyramidal neurons expressing calcium sensors.
Supplementary Note 1	Biochemical properties of YCs
Supplementary Note 2	Kinetics analysis
Supplementary Note 3	Combined electrophysiology and two-photon imaging.
Supplementary Note 4	Toxicity of YC-Nano in short-term expression.
Supplementary Note 5	Confocal imaging of the twitching behavior in zebrafish embryos.

*Note: Supplementary Videos 1–6 are available on the Nature Methods website.*

Supplementary Figure 1 | Ca²⁺ affinity of the YC-Nano. The normalized FRET signal was plotted against the logarithmic representation of the Ca^{2+} concentration. Fitted curve for the averaged data of three independent measurements is presented. The YC2.60 and YC3.60 series are shown in the upper and lower panel, respectively.
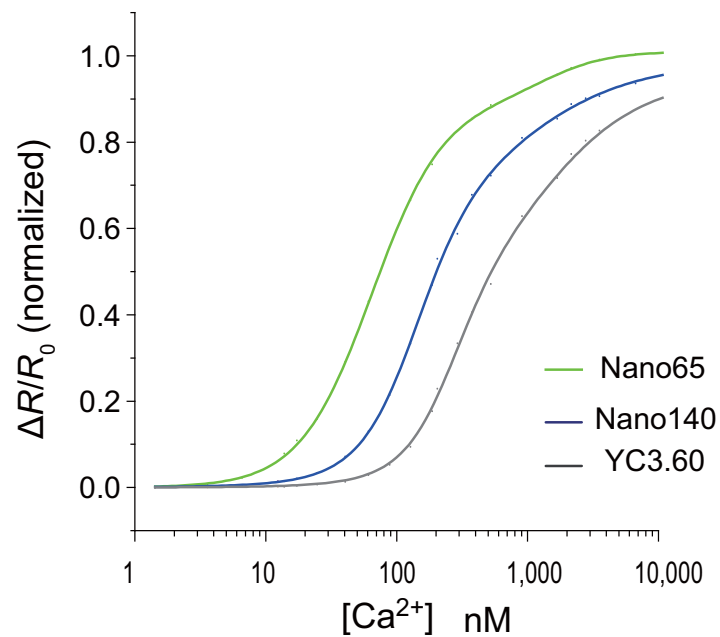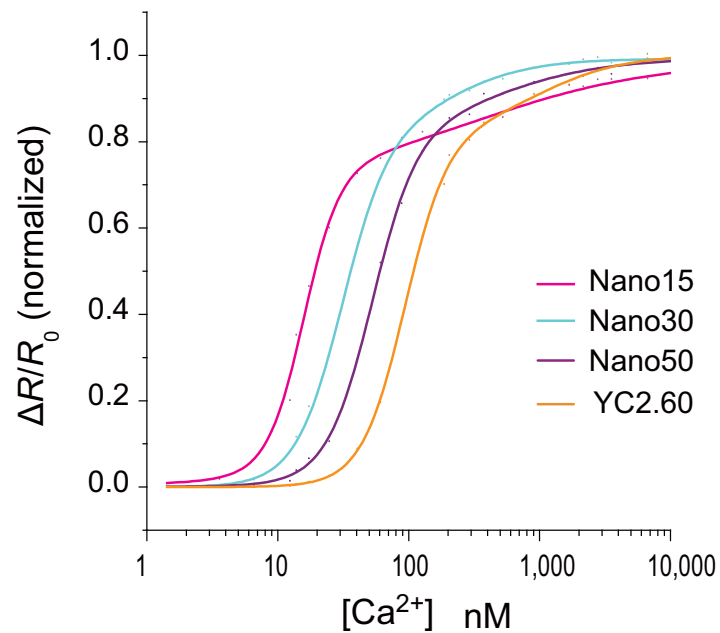
Supplementary Figure 2 | Relaxation rate constant (kobs) for YC3.60 or YC-Nano140 with Ca^{2+}. Association and dissociation rate constants (kon and koff) were determined by fitting to the equation $k_{obs} = k_{on} [Ca^{2+}] + k_{off}$. For details, see **Supplementary Note 2**.

Supplementary Figure 3 | Spectra for YC-Nano15. Normalized fluorescent spectra of YC-Nano15 in the absence of Ca^{2+} (cyan) or in the presence of a saturating concentration of Ca^{2+} (magenta). The emission spectrum of proteinase K-digested YC-Nano15 is indicated in gray. For details, see **Supplementary Note 1.**
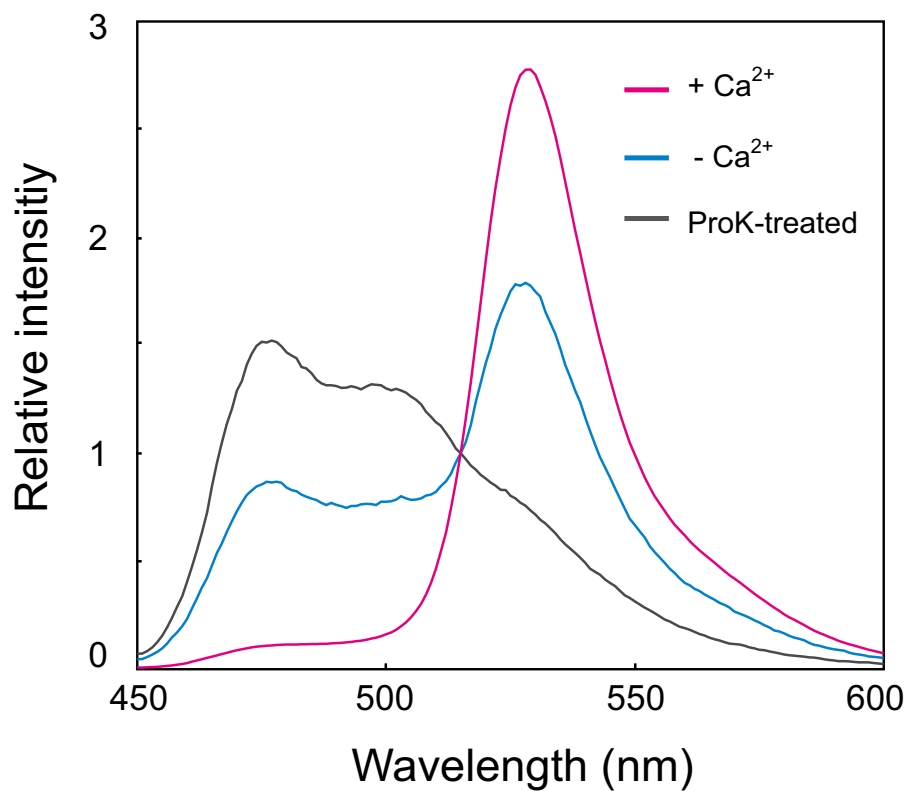
Supplementary Figure 4 | Growth rate and developmental time course of *D. discoideum* **cells expressing YC2.60 and YC-Nano15. (a-d)** Differential interference contrast images of cells before (**a, b**) and after (**c, d**) starvation. Note the rounded and elongated shapes characteristic of cells before and after starvation, respectively. (**e-j**) Development under semi-dry conditions. Aggregation stream (**e, f**) and low- (**g, h**) and high- (**i, j**) magnification views of the resulting fruiting bodies. (**k**) Doubling time of cells in the suspension culture.
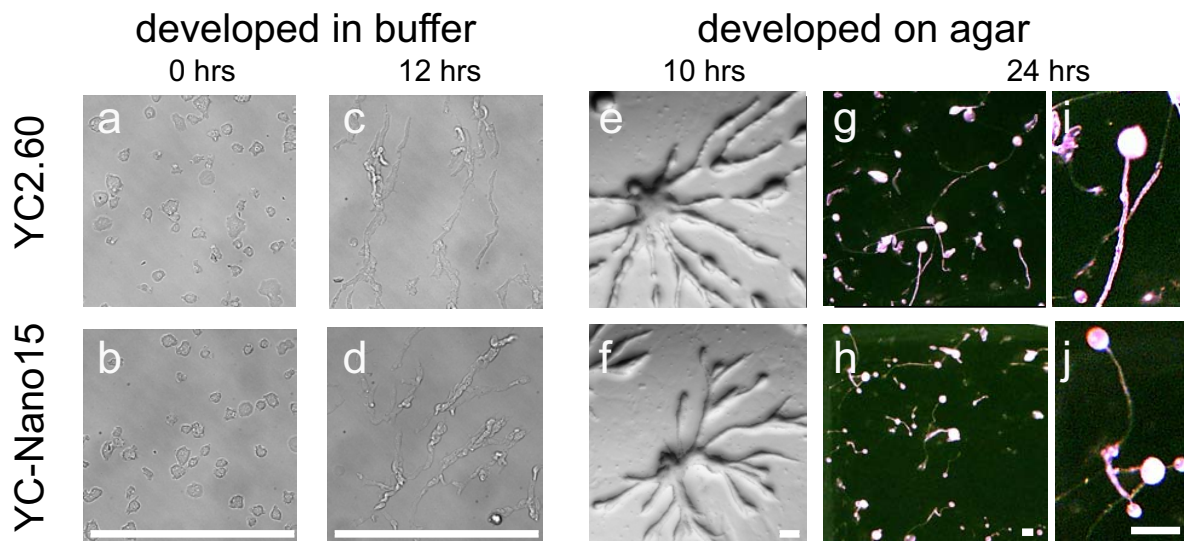
expressed gene	EGFP	YC2.60	YC-Nano15
doubling time (hrs)	8.1	8.3	8.1

Supplementary Figure 5 | Ca²⁺ imaging of spontaneous network activity in a 100,000-cell network. (a, b) Spiral-shaped intercellular signaling wave in a 100,000-cell network of *Dictyostelium discoideum* visualized by YC-Nano15. YFP (a) and YFP/CFP ratio images (b) in a 2 mm x 2 mm field of view. (c) The spatiotemporal wave pattern in the yellow inset of panel b is represented as a kymograph (every 15 seconds for 15 minutes). (d) Time course of the FRET signal change in the white box in b. See also Supplementary Video 2. Scale bar, 2 mm.
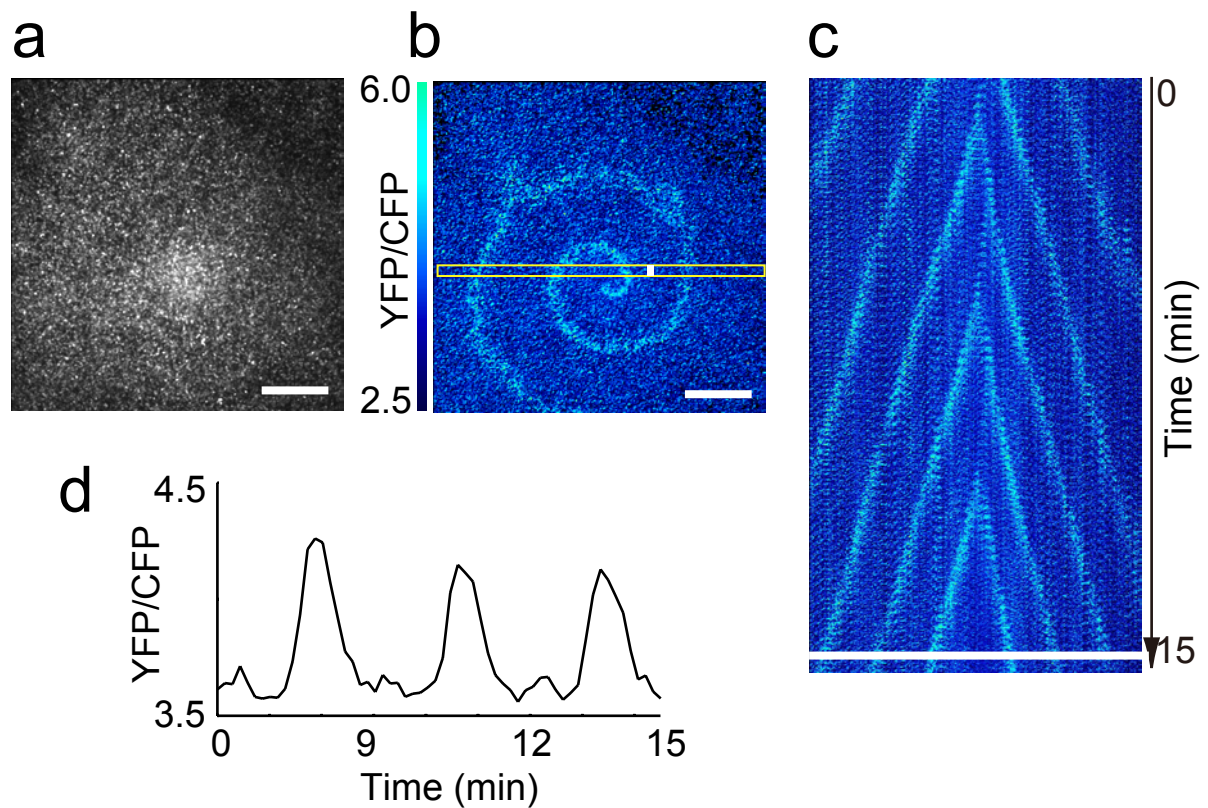
Supplementary Figure 6 | Aggregation waves of *Dictyostelium* **cells visualized with YC2.60.** (a, b) Spiral-shaped intercellular signaling wave in a 100,000-cell network of *Dictyostelium discoideum* visualized by YC2.60. a and b show YFP and YFP/CFP ratio images, respectively . (c) The spatiotemporal wave pattern in the yellow inset of panel b is represented as a kymograph (every 15 seconds for 15 minutes). (d) Time course of the FRET signal change in the white box in b. Scale bar, 1 mm..
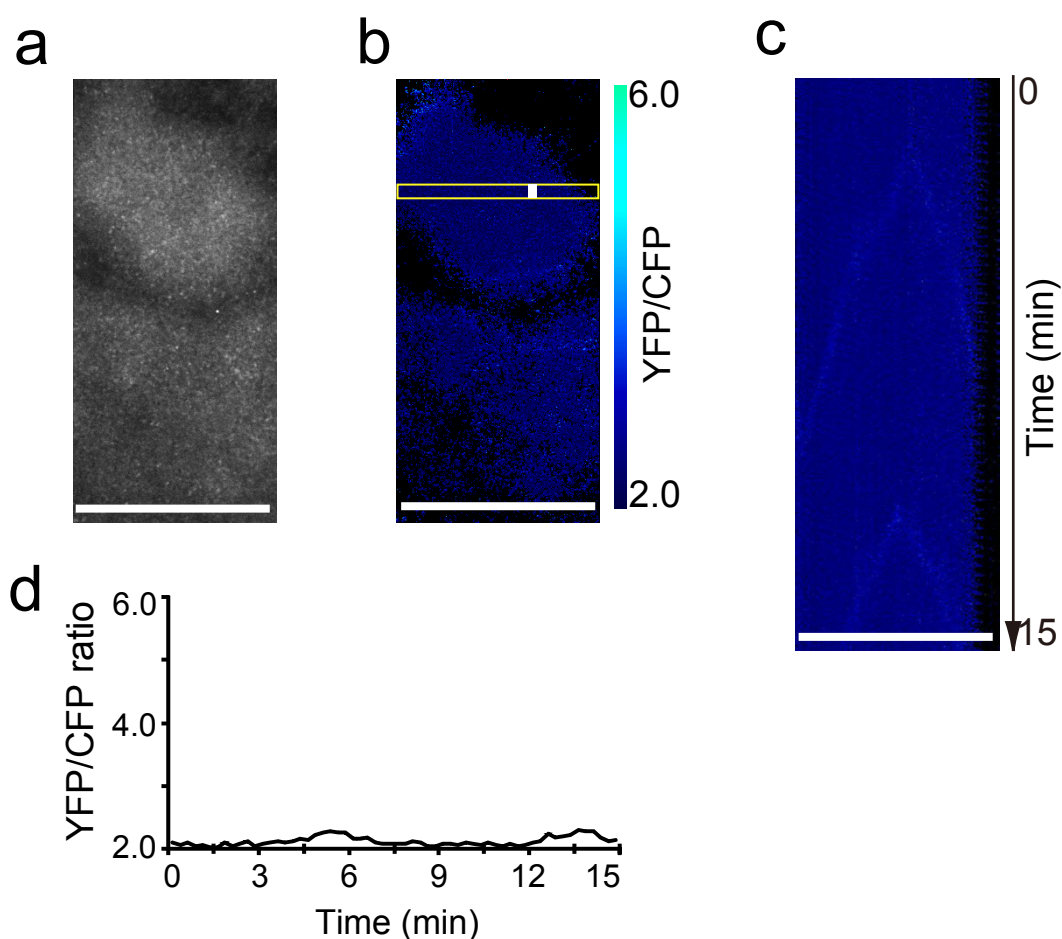
Supplementary Figure 7| YC3.60 and YC-Nano15 signals in response to trains of action potentials. (**a**) Maximum fluorescence intensity projection of a YC-Nano15-expressing pyramidal neuron, and expanded single z-section images within the white boxes. Bar, 5 μm. Line-scan images along the red line in response to 20 action potentials evoked at 20 Hz (arrowhead, stimulus onset). (**b**) Responses of YC3.60 (black) and YC-Nano15 (red) in layer 2/3 cortical pyramidal neurons to 1, 2, 5, and 10 action potentials evoked at 20 Hz (bar; stimulus period). $\Delta R/R_0$ traces averaged from 3 trials are shown.(**c**) Single action potential response detected with YC-Nano15 in samples from P17 and P72 mice. $\Delta R/R_0$ traces averaged from 3 trials are shown. Bar or arrow, stimulus timing.
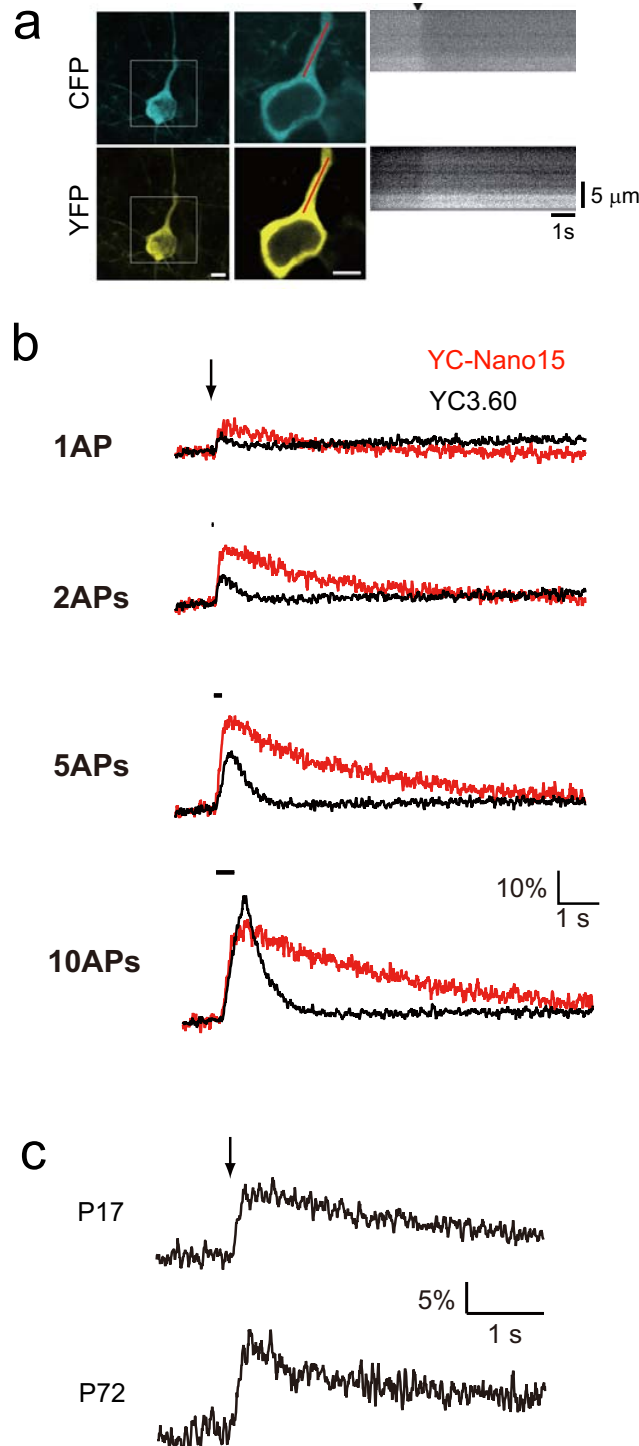
Supplementary Table 1 | Properties of new YC variants

	Dynamic range, %	R_{max}	R_{min}	K'_d, nM	Hill coefficient	Fraction, %
YC3.60	1,400	30	2	215.0	3.6	33
				779.6	**1.2**	**67**
YC-Nano140	1,300	28	2	**140.5**	**2.0**	**62**
(YC3.60 3GS)				754.1	0.9	38
YC2.60	1,300	28	2	**93.5**	**2.7**	**80**
				950.3	1.0	20
YC-Nano65	1,300	28	2	**64.8**	**1.6**	**90**
(YC3.60 4GS)				1441.3	1.8	10
YC-Nano50	1,250	27	2	**52.5**	**2.5**	**82**
(YC2.60 2GS)				403.8	1.0	18
YC-Nano30	1,250	27	2	**31.2**	**2.4**	**83**
(YC2.60 3GS)				204.8	1.3	17
YC-Nano15	1,450	31	2	**15.8**	**3.1**	**72**
(YC2.60 4GS)				320.2	0.6	28

Supplementary Table 2 | Electrophysiological properties of layer 2/3 pyramidal neurons expressing calcium sensors. All values are corrected for liquid junction potential (12 mV). There was no significant difference among the values from YCnano15-expressing cells, YC3.60-expressing cells and control cells (one-way ANOVA). [a] resting membrane potential. [b] input resistance. [c] threshold voltage for action potential generation. [d] amplitude of action potential measured from resting membrane potential. [e] half width of action potential.

Electrophysiological property		YCnano15 (n=14)	YC3.60 (n=7)	WT (n=5)	p-value
V_m[a]	(mV)	-81.4±6.5	-85.9±3.2	-81.2±11	0.33
R_m[b]	(MΩ)	209±59	-195±54	156±54	0.23
AP threshold[c]	(mV)	-46.2±5.4	-44.9±4.5	-42.9±6.9	0.51
AP amplitude[d]	(mV)	100±6.8	95.4±12	105±20	0.41
AP half width[e]	(ms)	2.46±0.58	3.69±2.3	1.97±0.68	0.063

Supplementary Note 1

Biochemical properties of YCs

In the present paper, we report different values for the dynamic range of Ca^{2+} detected from the values we reported previously (560%)[12] for YC2.60 and YC3.60, as well as different K_ds for Ca^{2+}. We attribute the difference to the greater purity of the recombinant proteins examined in this study. Here, to determine the dynamic range of the signal change in the indicators precisely, polyhistidine and biotin analog tags were attached to the YC proteins' N- and C-termini, respectively, and the proteins were sequentially purified by a Ni-NTA column and StrepTactin beads column, thereby only purifying the full-length recombinant proteins. On the other hand, the single-step purification with the Ni-NTA column used in the previous report resulted in a small amount of contamination with irregularly digested proteins, which interfered with the dynamic-range measurement.

After obtaining the highly purified YCs, we further determined the FRET efficiency of the YC-Nano. We calculated it to be 43% in the absence of Ca^{2+} and 93% in the presence of saturating Ca^{2+}, by the following equation:

$E = 1 - F_{DA}/F_D$ (eq. 1)

where E is the FRET efficiency, and F_{DA} and F_D are the fluorescence intensity of the donor in the presence and absence of the acceptor, respectively. F_D was obtained by measuring the fluorescence intensity of the YC-Nano after digestion with proteinase K (**Supplementary Fig 3**). Trypsin digestion gave an almost identical value for the FRET efficiency (data not shown).

Supplementary Note 2

Kinetics analysis

To understand how the elongated linker affected the kinetic properties, we measured the

Ca^{2+}-association kinetics by stopped-flow photometry. Due to the feasibility of

controlling the Ca^{2+} concentration above the 100 nM range, we measured the tau for the

Ca^{2+} association reaction from zero Ca^{2+} to various Ca^{2+} concentrations for YC3.60 and

YC3.60 modified with the elongated linker (3GS) (+4; Gly-Gly-Gly-Ser). By fitting the

observed data to the equation, $k_{obs} = k_{on} [Ca^{2+}] + k_{off}$, we obtained comparable

dissociation rate constants for YC3.60 and YC-Nano140 (0.34 and 0.33 s^{-1},

respectively), and an increased rate constant for the on reaction for YC-Nano140 (1.33

$\times 10^6$ $M^{-1}s^{-1}$ for YC3.60 and 2.36 $\times 10^6$ $M^{-1}s^{-1}$ for YC-Nano140). These data nicely

account for the increased Ca^{2+} affinity of the molecule containing the elongated linker,

because the apparent dissociation constant (K_d) calculated from the following equation

$K_d = k_{off} / k_{on}$, where we obtained K_ds for YC3.60 and YC-Nano140 of 255 nM and 139

nM respectively, were comparable to the values obtained by the independent Ca^{2+}

titration experiment (high-affinity fraction K_d = 215 and 140 nM for YC3.60 and

YC-Nano140, respectively (see **Supplementary Table 1**). These results suggest that

linker elongation accelerates the Ca^{2+}-induced conformational change of CaM-M13,

which might be sterically restricted by the shorter linker.

Although we would like to measure the k_{off} of YC2.60 and its high affinity

variants such as YC-Nano15, we could not do it because it was very difficult to

precisely control free Ca^{2+} concentration at around few tens of nM as far as we used

EGTA (K_d for Ca^{2+} = 151 nM in 0.1 M ionic strength, pH 7.2 at 25 ºC). For this purpose,

much stronger Ca^{2+} chelator with a smaller K_d value was required. However there is no such Ca^{2+} chelator available now. Therefore it was almost impossible to experimentally determine the k_{on} and k_{off} values of YC2.60 and its high affinity variants. Because YC3.60 have an affinity-lowering mutation, E104Q, in the CaM moiety, it would be reasonable to assume that k_{off} of YC2.60 and its variants were much smaller than that of YC3.60, while their k_{on}s were comparable. The slow decay kinetics of YC-Nano15 in neurons (**Fig. 2**, **Supplementary Fig. 7**, see **Supplementary Note 3**) could be explained by the smaller k_{off} of YC-Nano15 than that of YC3.60.

Supplementary Note 3

Combined electrophysiology and two-photon imaging.

To verify the properties of the high-affinity YCs in living neurons, we generated recombinant adenoviruses carrying YC-Nano15 and YC3.60 cDNA. The YCs were introduced into mouse brain by the adenoviral vectors on embryonic day 14, which expressed them under the control of the CAG promoter, according to the method described elsewhere (Y. Yamada *et al.*, manuscript in preparation). At 15-72 postnatal days (P15-P72), an acute slice was prepared and subjected to a combination of electrophysiology and two-photon imaging. Electrophysiological properties of patched layer 2/3 pyramidal neurons are as follows; a resting potential of -85.9 ± 3.2 mV (YC3.60, n = 7), -81.4 ± 6.5 mV (YC-Nano15, n = 14) and -81.2 ± 11 mV (control, n = 5), an input resistance of 195 ± 54 MΩ (YC3.60, n = 7), 209 ± 59 MΩ (YC-Nano15, n = 14) and 156 ± 54 MΩ (control, n = 5), and a threshold for action potential generation of -44.9 ± 4.5 mV (YC3.60, n = 7), -46.2 ± 5.4 mV (YC-Nano15, n = 14) and -42.9 ± 6.9 mV (control, n = 5), suggesting that the YC-Nano15 as well as YC3.60 do not cause specific side effects at the expression level achieved by the CAG promoter (**Supplementary Table 2**). Current pulses were injected into the soma of whole-cell-patched layer 2/3 pyramidal neurons, and the fluorescence intensity change was line-scanned at the apical dendrite (**Supplementary Fig. 7a**). To correlate the number of AP and FRET signal changes, a series of current-triggered trains of 1, 2, 5, or 10 action potentials were elicited at a frequency of 20 Hz. The averaged $\Delta R_{YC3.60}$ (P15 mice, n = 5) was 5.5 ± 1.2 for the single action potential, 9.0 ± 1.5 for two, 20.6 ± 6.8 for five, and 41.4 ± 12.9 for ten action potentials (**Fig. 2a**). That of YC-Nano15

(ΔR_{Nano15} at P17 or P19, n = 7) was 10.4 ± 1.9 for the single, 16.3 ± 3.7 for two, 26.4 ± 7.7 for five, and 31.8 ± 11.6 for ten APs **(Fig. 2a)**. The SNR for 1, 2, 5, and 10 APs was 2.9, 4.6, 10.1, and 21.0 for YC3.60, and 4.2, 5.9, 9.5, and 11.4 for YC-Nano15, indicating that YC-Nano15 has a higher detection sensitivity for the subtle Ca^{2+} transients associated with a single or small number of APs.

As expected, YC-Nano15 is not suitable for the detection of the large Ca^{2+} transients triggered by high-frequency stimulus, due to the signal saturation and the slow decay time (3-4 sec) (more than 10 APs at 20 Hz or trains of single APs at 2 Hz **Fig. 2b**). It would be reasonable to use YC-Nanos for the detection of non-bursting Ca^{2+} spikes of less than 1 Hz, similar to D3cpV, which possesses similar properties, including the single-AP sensitivity, saturating frequency, and slow decay time[4].

The single-AP sensitivity of YC-Nano15 was also verified in neurons subjected to long-term expression. The ability of YC-Nano15 to detect a single AP response was not affected in the cortical neurons from an acute slice of P72 mice (n = 3, **Supplementary Fig. 7c**), suggesting that the long-term expression of high-affinity YC is not very toxic under our experimental conditions.

Supplementary Note 4

Toxicity of YC-Nano in short-term expression.

To examine the short-term effect of YC-Nano, we injected different amounts of the indicators into zebrafish embryos, and checked the embryos' viability (**Fig A**, n > 90 for each experimental condition). Their viability was not severely affected at the low expression level (less than 10 μM at 24 hpf), where ratiometric imaging can be easily achieved. Less viability at higher loading level (more than 10 μM) was evident in Venus-loaded embryos suggesting non-specific effect of protein injection. However, the toxic effect in YC-Nano50 and YC3.60 might be partially resulted from interference of the CaM-M13 peptide domains with endogenous signaling pathways as reported elsewhere[4, 6].
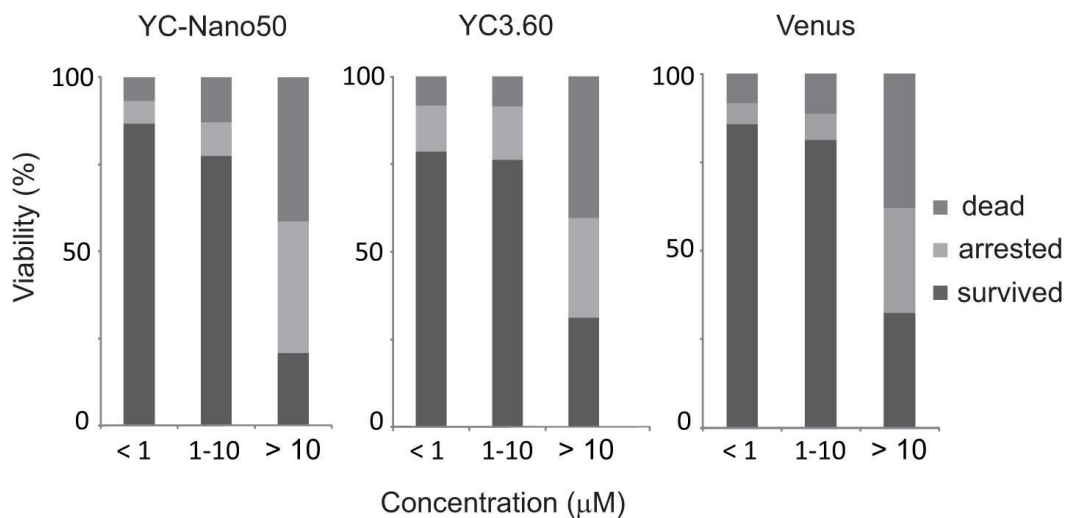
Fig. A. Viability of zebrafish embryos injected with different amounts of YCs.

Supplementary Note 5

Confocal imaging of the twitching behavior in zebrafish embryos.

At 17 hours post fertilization (hpf), zebrafish embryos initiated a spontaneous twitching behavior[24] that persisted until 30 hpf with decreasing frequency from 1 to 0.1 Hz (**Supplementary Video 4**). We found that YC-Nano50 was the best indicator to detect cellular activity in these living fish embryos. Cells loaded with high-affinity YC (Nano15) showed small donor signals compared with acceptor signals, which is not ideal for FRET measurement. This was partially because of cross-excitation of the YFP with the 458-nm laser line that is commonly used in confocal microscopes, and partially due to the large FRET signals, reflecting the relatively high Ca^{2+} levels, especially in a subset of cells (neurons) under resting conditions. On the other hand, cells loaded with low-affinity YC (YC3.60) showed donor signals in neurons (estimated to have a high Ca^{2+} level), but the FRET change was small due to the sub-optimal Ca^{2+} affinity (**Fig. 3**).

For confocal observation of the Ca^{2+} transients during the spontaneous twitching behavior, purified YC-Nano50 protein was injected into fertilized eggs (approx. final concentration of 5 μM), and the Ca^{2+} transients in the spinal neurons and muscles were imaged simultaneously by a widely used confocal microscopy method. We detected bilaterally alternating firing of a subset of spinal cord neurons (**Fig. 3** and **Supplementary Video 4**). Simultaneous with the neuronal firing, we also detected [Ca^{2+}] increases in the fast and smooth muscle. These results clearly revealed the spatio-temporal firing pattern of the cellular network involved in the spontaneous twitching behavior of a living animal. We also found that our high-affinity indicator

revealed different FRET signals depending on the cell type: high FRET signals for the epidermis and spinal neurons, and low FRET signals for fast and smooth muscles, suggesting different basal [Ca^{2+}] levels in living embryos. These results strongly support the idea that optimization of the indicator's properties, for the organism, the cell type, and the context of the stimulation, is essential for successful live-cell imaging.

References

24. Saint-Amant, L., & Drapeau, P., *J. Neurobiol*. **37**(4) 622-632 (1998)